Journal of Alloys and Compounds 517 (2012) 40–44

Contents lists available at SciVerse ScienceDirect

Journal of Alloys and Compounds

journal homepage: www.elsevier.com/locate/jallcom

Laser-assisted atom probe tomography investigation of magnetic FePt nanoclusters: First experiments

E. Folcke [a], R. Lardé [a], J.M. Le Breton [a,*], M. Gruber [a], F. Vurpillot [a], J.E. Shield [b], X. Rui [b], M.M. Patterson [c]

[a] Groupe de Physique des Matériaux, UMR CNRS 6634, Université de Rouen, 76801 Saint Etienne du Rouvray, France
[b] Department of Mechanical & Materials Engineering, Nebraska Center for Materials and Nanoscience, University of Nebraska, N104 WSEC, Lincoln, NE 68588, USA
[c] Department of Physics, University of Wisconsin-Stout, Menomonie, WI 54751, USA

ARTICLE INFO

Article history:
Received 5 August 2011
Received in revised form
25 November 2011
Accepted 26 November 2011
Available online 17 December 2011

Keywords:
FePt nanoclusters
Atom probe tomography

ABSTRACT

FePt nanoclusters dispersed in a Cr matrix have been investigated by laser-assisted atom probe tomography. The results were analysed according to simulated evaporation experiments. Three–dimensional (3D) reconstructions reveal the presence of nanoclusters roughly spherical in shape, with a size in good agreement with previous transmission electron microscopy observations. Some clusters appear to be broken up after the evaporation process due to the fact that the Cr matrix has a lower evaporation field than Fe and Pt. It is thus shown that the observed FePt nanoclusters are chemically homogeneous. They contain Fe and Pt in equiatomic proportions, with no core–shell structure observed.

1. Introduction

The field of magnetic nanoclusters has far-reaching technological implications, from disk drive technology to high-energy permanent magnets. Due to their large magnetocrystalline anisotropy, FePt nanoclusters with the $L1_0$ structure are among the more promising candidates for high density recording media [1,2]. However, most preparation methods produce the disordered, magnetically soft A1 phase and require additional processing which can introduce contaminants or result in particle agglomeration [3]. Experiments and simulations indicate that phase transformation from A1 to $L1_0$ may be kinetically inhibited in nanoclusters smaller than 4 nm [4]. A method that allows formation of nanoclusters already in the $L1_0$ state, without the need for post-formation thermal treatments, would not only save significant processing cost, it would increase information storage density for recording media.

Recently, it has been shown that synthesis of FePt nanoclusters via inert gas condensation has yielded direct formation of partially ordered $L1_0$ structure [5,6]. Recent work has examined the effects of plasma characteristics on the early stages of order in the formation $L1_0$ FePt nanoclusters via inert gas condensation [7]. The results indicate that controlled ion density directly impacts the early stages of FePt nanocluster ordering.

It is critical to have an understanding of the relationship between cluster size and shape and the magnetic behaviour. In particular, it is important to understand surface effects as the cluster size decreases, as the changes in magnetism associated with the broken symmetry of surface atoms become non-negligible. Additionally, faceting along different planes alters surface effects—and magnetism—as the cluster shape changes.

With this aim, FePt nanoclusters produced via inert gas condensation were investigated by the laser assisted atom probe tomography (LAAPT). This technique offers an ultrahigh spatial resolution (depth resolution ~ 0.1 nm) and provides a powerful method to observe both structure and chemical composition at the atomic scale [8]. In this paper, we present the first LAAPT investigation of FePt nanoclusters. The results (3D reconstructions and concentration profiles) are discussed in relation with the field evaporation process that has been simulated prior to the experiment.

2. Experimental

FePt clusters were created by inert gas condensation [7] from a composite sputtering target consisting of Pt pieces in an Fe target, biased at 360 V (150 W), drawing 330 mA of plasma current (Fig. 1). Argon introduced into the source chamber created pressures of between 18 and 72 Pa. The deposition chamber pressures of between 0.27 and 0.93 Pa were controlled via argon flow rates. Depending on the processing conditions, nanoclusters with different shapes were obtained, as shown by the high resolution transmission electron microscopy (HRTEM) images in Fig. 2. The HRTEM imaging was accomplished on clusters directly deposited onto carbon support grids using a Tecnai G2F20 operating at 200 kV.

Samples for LAAPT investigation were obtained by depositing FePt clusters in a Cr matrix on a pre-patterned substrate consisting of an assembly of flat-topped Si

* Corresponding author. Tel.: +33 2 32 95 50 39; fax: +33 2 32 95 50 32.
E-mail address: jean-marie.lebreton@univ-rouen.fr (J.M. Le Breton).

0925-8388/$ – see front matter © 2011 Elsevier B.V. All rights reserved.
doi:10.1016/j.jallcom.2011.11.134

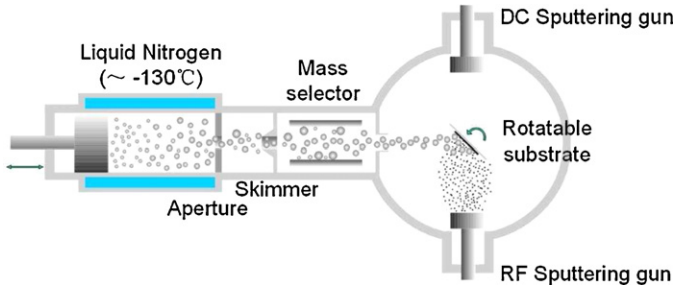

Fig. 1. Schematic picture of nanocluster fabrication system. The formation chamber is on the left, inside the cooled region; the deposition chamber, on the right, nears the rotatable substrate. The FePt target is the leftmost object in the chamber.

(1 0 0) posts. The silicon posts (100 μm height, 100 μm^2 area) were obtained by patterning a Si wafer with the Bosch process [9]. According to the processing conditions, spherical nanoclusters are expected.

Atom probe tomography is based on the field evaporation of surface atoms as ions, and their identification by time of-flight mass spectrometry. The high electric field required (a few tens of V/nm) is obtained by applying a high voltage to the sample prepared in the form of a sharply pointed needle (tip radius less than 50 nm). The tip is biased at a high positive DC voltage V_o in the 2–10 kV range and cooled to low temperatures (20–80 K). The vacuum in the analysis chamber is usually in the 10^{-8} Pa range. Surface atoms are then field-evaporated by means of high-frequency (100 kHz) laser pulses superimposed on the DC voltage V_o [10] The femtosecond laser pulsed system used is an amplified ytterbium-doped laser (AMPLITUDE SYSTEM s-pulse) with a pulse length of 350 fs. The evaporated atoms are collected by a time-resolved position detector located in front of the sample. It allows time-of-flight measurements of each ion and to record its impact position. This information allows the chemical nature of evaporated ions to be deduced and the position from which atoms originate at the tip surface to be calculated. The lateral positions of atoms at the surface of the tip sample are obtained from a back projection of ion impacts coordinates on the position sensitive detector. The depth position is deduced from the order of detection of atoms [11]. The sample is field-evaporated atom per atom and a 10^4 nm^3 typical volume is collected in a few hours. After the 3D reconstruction of the analysed volume, the spatial distribution of atoms is observable at the atomic scale in the real space. From the data set of the 3D reconstruction, chemical composition or concentration depth profiles can be calculated everywhere in the analysed volume.

3. Results and discussion

3.1. Modelling of the atom probe experiment

In atom probe tomography, the specimen is evaporated atom per atom while the impact positions of the projected ions on a detector are determined. The tomographic reconstruction is calculated using a back projection algorithm that takes the geometric features of the sample into account. This procedure, well adapted to homogeneous materials, faces limitations when analysing nanostructured materials. The end form of the specimen changes continuously during evaporation, depending on the structure of the analysed material, the experimental conditions and the nature of elements present in the different phases. This can give rise to changes in the projection law between the detector and the specimen surface. Reconstruction aberrations are therefore often observed and can bias measurements [12]. In order to overcome this, a modelling approach was developed [13–15]. To understand the effects of nanostructure on the back projection algorithm, the gradual evolution of the tip under field evaporation is modelled numerically. This evolution is obtained by calculating the electric field above the surface of the tip subjected to the DC voltage, and by determining the induced sequence of evaporation. To obtain data corresponding to the result of an experimental analysis, the ion trajectories are calculated between the tip and a virtual detector. For each surface atom the electric field is measured at the surface of the corresponding Wigner Seitz cell. Field evaporation is the transition of a surface atom into an n-times charged ion under the influence of the external electric field (in the range 10–100 V/nm). This process is thermally activated and described by an Arrhenius law [16]. The evaporation sequence is determined step-by-step to determine which atom to evaporate next. We assume in a first approximation that the evaporation fields of elements in an alloy are very close to the evaporation fields of the pure metals. Using classical laws, ion trajectories in the field distribution are calculated and the tip-to-image transfer function is deduced. More details about the model can be found in previous publications [13–15].

The Cr—FePt field emitter is represented as a stack of atoms in the form of a cylinder terminated by a hemispherical cap of radius R = 16 nm. The modelled tip is composed of a pure Cr matrix with spherical and homogeneous $Fe_{0.5}Pt_{0.5}$ precipitates of 3 nm diameter, in agreement with TEM analysis. The global composition corresponds to the values measured by LAAPT: 6.4% Fe and 6.4% Pt in Cr The crystalline structure of both matrix and precipitates is fcc. The evaporation fields are: 29 V/nm for Cr, 35 V/nm for Fe, and 45 V/nm for Pt. The particles are placed randomly (8.9×10^{18} precipitates/cm^3). An image of the initial distribution of the FePt precipitates in the Cr matrix corresponding to the modelled tip is shown in Fig. 3a. The image is perpendicular to the modelled tip axis.

A 2D projection of a reconstructed volume obtained after the simulated evaporation sequence is shown in Fig. 3b. The 2D projection is perpendicular to the tip axis. Only the Fe and Pt atoms are shown, revealing the position of the clusters. The crossed lines that appear in the figure correspond to zone axes. They are due to the fact that both matrix and precipitates have the same fcc crystalline structure. The Fe and Pt atoms appear in the same

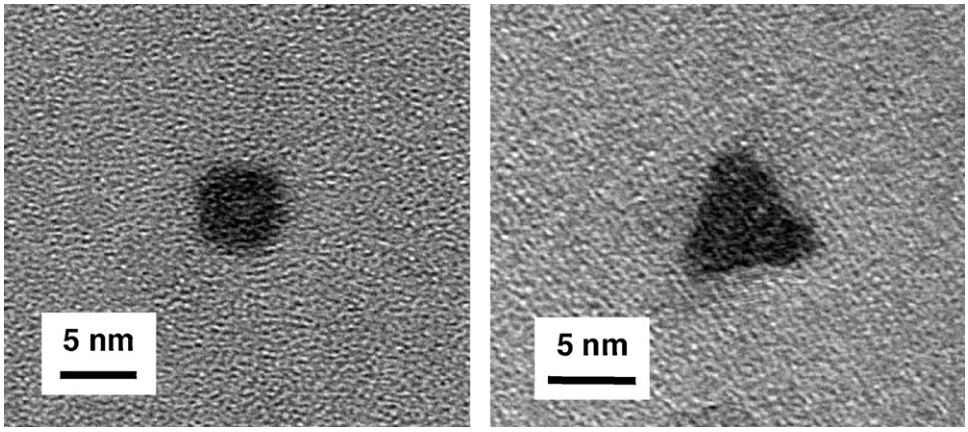

Fig. 2. HRTEM images of FePt single crystals obtained from different experimental conditions: (left) spherical cluster and (right) faceted cluster.

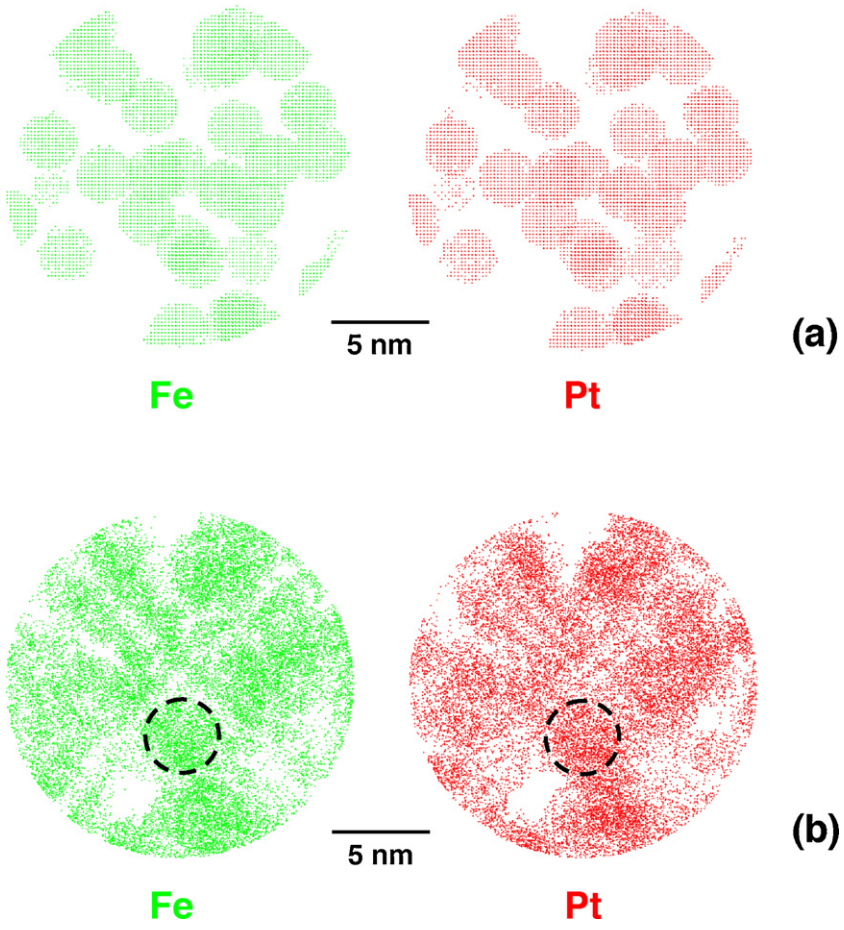

Fig. 3. 2D projections of a reconstructed volume perpendicular to the direction of the simulated analysis. (a) FePt nanoclusters (diameter: 3 nm) in the modelled tip before simulation: the distributions of Fe and Pt are equivalent. (b) Distribution of Fe and Pt atoms after simulation.

regions, in precipitates with no well-defined shape. The reconstruction suggests that, in some regions, reconstructed nanoclusters could be roughly spherical (dotted circles in Fig. 3b), with a size less than about 4 nm, which is a little larger than in the modelled material. Other clusters appear to be broken up after the evaporation process. The matrix/precipitates interfaces are not well defined.

Concentration profiles across FePt nanoclusters, along the tip axis, were obtained. An example is shown in Fig. 4. The Fe and Pt profiles are similar, and show that these elements are present on a length of about 4 nm, in agreement with the apparent size observed in Fig. 3a. The matrix/nanocluster interfaces are not sharp, being extended to more than 1 nm. This can be attributed to the fact that the evaporation field of the Cr matrix is lower than those of Fe and Pt. In the centre of the FePt clusters, the $Fe_{50}Pt_{50}$ composition is obtained, in very good agreement with the concentrations in the modelled tip.

These results show that the evaporation of a sample constituted of FePt spherical nanoclusters in a Cr matrix leads in the reconstructed volume to a mixing of Fe and Pt atoms with Cr. This artificial mixture is due to the difference in the evaporations field between the matrix and the nanoclusters. The apparent size of the observed nanoclusters, that have no well-defined shape, is larger than their real size in the starting material. Some precipitates appear to be broken up. However, in the reconstructed volume, and although the Fe and Pt atoms have different evaporation fields, the Fe concentration profiles correspond to the Pt ones. Consequently, the measured composition of the FePt precipitates is equiatomic. The reconstructed nanoclusters thus appear to be homogeneous, like in the starting materials.

3.2. Experimental analysis

A 3D reconstructed volume of the investigated specimen is shown in Fig. 5. The FePt nanoclusters are represented in yellow and evidenced by isoconcentration surfaces (threshold: 20% Fe and 20% Pt). The image reveals the FePt nanoclusters embedded in the Cr matrix. The clusters appear spherical in shape, with a size distribution between 1 and 5 nm, in good agreement with HRTEM analysis. The reconstruction does not reveal if some clusters are faceted, as the shape of the clusters is not regular. The measured atomic composition of the nanoclusters is in very good agreement with the nominal composition, the same atomic content being obtained for Fe and Pt. The measured atomic global concentrations are close to 6.4% Fe, 6.4% Pt and 87.2% Cr.

A 2D projection of a reconstructed volume obtained after the experimental analysis is shown in Fig. 6. The 2D projection is perpendicular to the tip axis. The positions of the Fe and Pt atoms clearly reveal the nanoclusters. However, the shape of the observed precipitates is neither regular nor homogeneous. Some precipitates appear to be broken up. However, some other precipitates seem to be roughly spherical, as indicated by the dotted lines in the figure. The observed nanoclusters appear to be size distributed. The matrix/precipitate interfaces are diffuse, in agreement with the differences in the evaporation field of the Fe, Pt and Cr elements.

An enlarged view of a region around a FePt nanocluster (Fig. 7) shows that the distributions of Fe and Pt atoms in the cluster

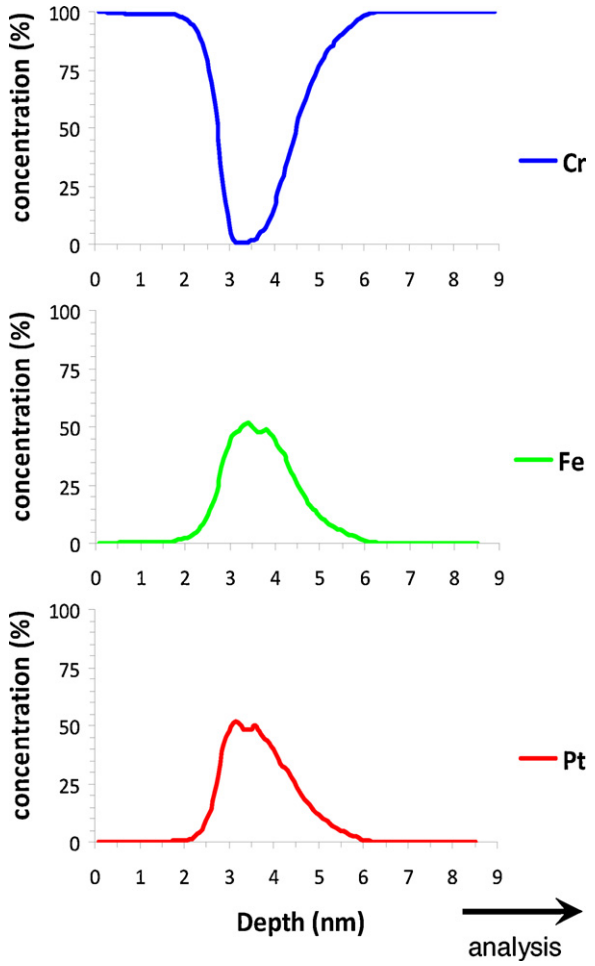

Fig. 4. Cr, Fe and Pt concentration profiles in a volume across a FePt cluster, obtained from the simulated analysis. The profiles are along the modelled tip axis.

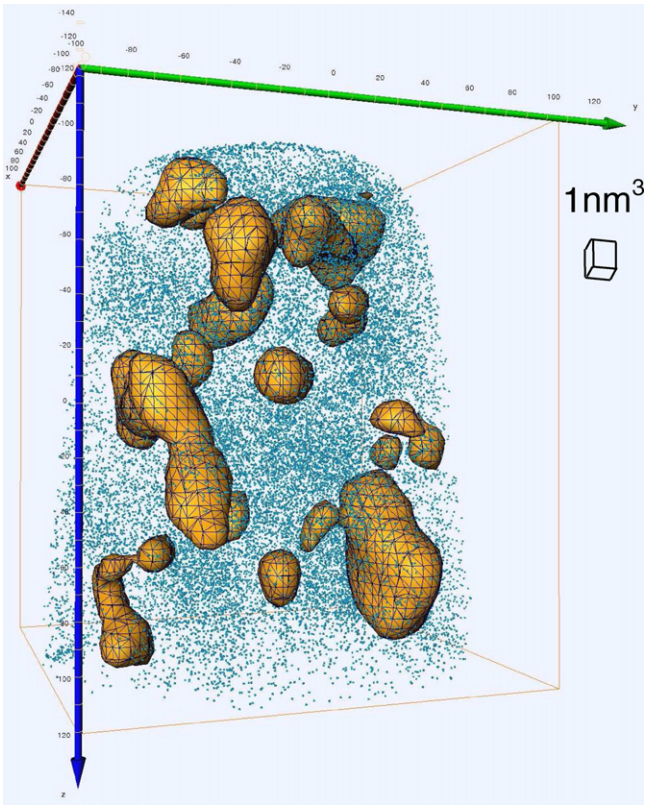

Fig. 5. 3D reconstruction image of FePt nanosized clusters embedded in a Cr matrix. The analysed volume is 20 nm × 20 nm × 25 nm. The nanoparticles of FePt are evidenced by isoconcentrations surfaces, in yellow (threshold: 20% Fe and 20% Pt). (For interpretation of the references to colour in this figure legend, the reader is referred to the web version of the article.)

are comparable. No core–shell atomic distribution is observed within the cluster. This is revealed as well on the concentration profiles (Fig. 8). Thus, the experimental analysis (reconstructed volumes and concentration profiles) reveals FePt nanoclusters with an equiatomic composition. According to the simulated experiments, this indicates that the FePt clusters in the investigated sample are chemically homogeneous, with a size distribution that extends from 1 to 5 nm.

It appears that the reconstruction does not reveal if the clusters are spherical or faceted. Moreover, some clusters appear to be broken up after the evaporation process. These effects are attributed to the fact that Cr has a lower evaporation field than those of Fe and Pt. Such a difference can also explain the fact that Cr is detected inside the FePt nanoclusters. In this case, some Cr atoms from the matrix can be evaporated together with Fe and Pt atoms from the nanoclusters, leading to an artificial Cr/FePt mixing, as observed in Fig. 8.

Thus, to get a more accurate analysis, one must consider the nature of the matrix. A matrix with an evaporation field higher

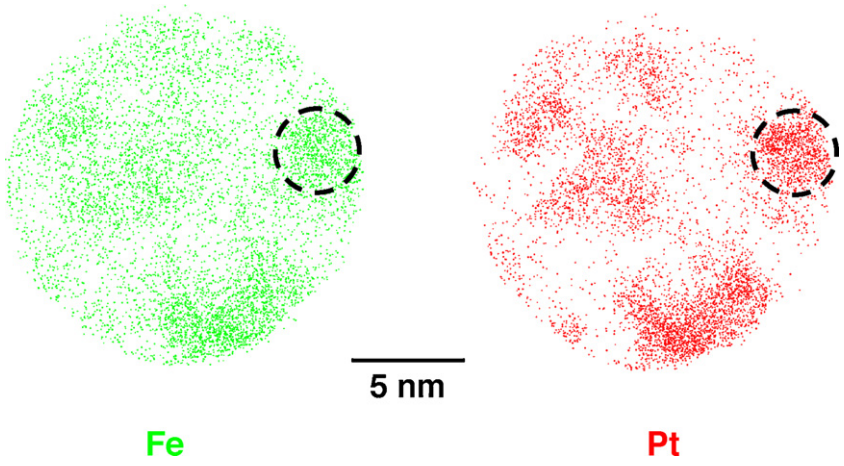

Fig. 6. 2D projection of a reconstructed volume perpendicular to the direction of the TAP analysis, showing the distribution of Fe and Pt atoms.

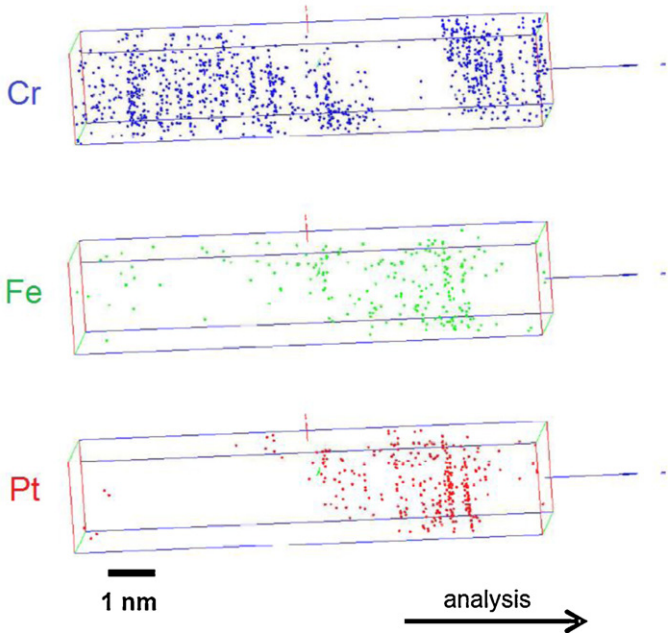

Fig. 7. 3D-reconstruction of a volume around a FePt cluster.

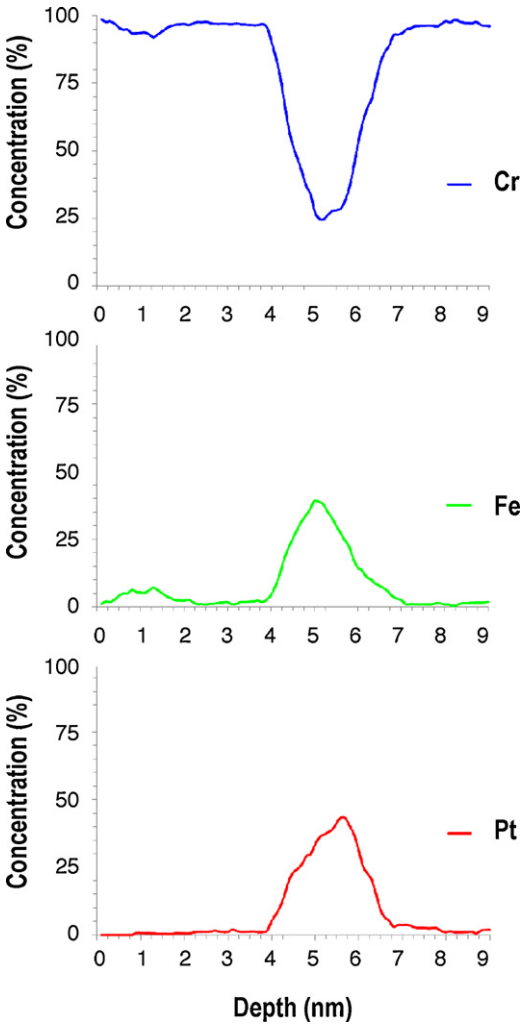

Fig. 8. Cr, Fe and Pt concentration profiles in a volume across a FePt cluster, obtained from the experiment. The apparent mixing of FePt with Cr is due to the difference between the evaporation field of Cr with those of Fe and Pt (see text).

than that of the clusters could avoid perturbation effects during the evaporation sequence. From that point of view, specimens consisting of FePt nanoclusters in a *W* matrix (the evaporation field of *W* being 52 V/nm) could allow more precise characterisation of the cluster shape.

4. Conclusion

FePt nanoclusters dispersed in a Cr matrix have been investigated by atom probe tomography, allowing a direct observation of their chemical structure. The results reveal, in agreement with the simulations of the evaporation sequence, that the clusters are chemically homogeneous, and no core–shell structure was observed. Fe and Pt atoms are present throughout the clusters in equiatomic proportions. Some observed clusters are roughly spherical in shape, with a size that is in good agreement with electron transmission microscopy observations. However, the reconstruction does not reveal if some clusters are faceted. This is due to the fact that Cr has a lower evaporation field than Fe and Pt. These results indicate that atom probe tomography allows a direct observation of the chemical structure of the FePt nanoclusters.

Acknowledgements

This work is supported by the IGERT program on magnetic materials between the Institute for Materials Research (IMR) at the University of Rouen and the University of Nebraska-Lincoln. Research at the University of Nebraska-Lincoln was supported by the National Science Foundation's Materials Research Science and Engineering Center (MRSEC) program by grant no. DMR 0820521.

References

[1] D.J. Sellmyer, C.P. Luo, M.L. Yan, Y. Liu, IEEE Trans. Mag. 4 (2001) 1286–1291.
[2] Y.F. Xu, M.L. Yan, D.J. Sellmyer, J. Nanosci. Nanotechnol. 7 (2007) 206–224.
[3] X. Rui, Z.G. Sun, Y. Xu, D.J. Sellmyer, J.E. Shield, J. Magn. Magn. Mater. 21 (2008) 2576–2583.
[4] R.V. Chepulskii, W.H. Butler, Phys. Rev. B 13 (2005) 134205 (18 pp.).
[5] M.M. Patterson, X. Rui, X.Z. Li, J.E. Shield, D.J. Sellmyer, Mater. Res. Soc. Symp. Proc. 1087 (2008) V08.
[6] J.M. Qiu, J.P. Wang, Adv. Mater. 19 (2007) 1703–1706.
[7] M.M. Patterson, A. Cochran, J. Ferina1, X. Rui, T.A. Zimmerman, Z. Sun, M.J. Kramer, D.J. Sellmyer, J.E. Shield, J. Vac. Sci. Technol. B 28 (2010) 273–276.
[8] D. Blavette, B. Deconihout, A. Bostel, J.M. Sarrau, M. Bouet, A. Menand, Rev. Sci. Instrum. 64 (1993) 2911–2919.
[9] A.A. Ayon, R. Braff, C.C. Lin, H.H. Swain, M.A. Schmidt, J. Electrochem. Soc. 146 (1999) 339–349.
[10] B. Gault, F. Vurpillot, A. Vella, M. Gilbert, A. Menand, D. Blavette, B. Deconihout, Rev. Sci. Instrum. 77 (2006) 043705 (8 pp.).
[11] P. Bas, A. Bostel, B. Deconihout, D. Blavette, Appl. Surf. Sci. 298 (1995) 87–88.
[12] M.K. Miller, A. Cerezo, M.G. Hetherington, G.D.W. Smith, Atom Probe Field Ion Microscopy, Oxford Science, Oxford, 1996.
[13] F. Vurpillot, A. Bostel, D. Blavette, J. Microsc. 196 (1999) 332–336.
[14] F. Vurpillot, A. Bostel, D. Blavette, Ultramicroscopy 89 (2001) 137–144.
[15] F. Vurpillot, M. Gruber, S. Duguay, E. Cadel, B. Deconihout, AIP Conf. Proc. 1176 (2009) 175–180.
[16] E.W. Müller, Phys. Rev. 102 (1956) 618–624.